 CMES, vol.28, no.2, pp.109-125, 2008

A Smoothed Finite Element Method (SFEM) for Linear and Geometrically Nonlinear Analysis of Plates and Shells

X.Y. Cui[1,2], G. R. Liu[2,3], G. Y. Li[1], X. Zhao[2], T.T. Nguyen[2] and G.Y. Sun[1]

Abstract: A smoothed finite element method (SFEM) is presented to analyze linear and geometrically nonlinear problems of plates and shells using bilinear quadrilateral elements. The formulation is based on the first order shear deformation theory. In the present SFEM, the elements are further divided into smoothing cells to perform strain smoothing operation, and the strain energy in each smoothing cell is expressed as an explicit form of the smoothed strain. The effect of the number of divisions of smoothing cells in elements is investigated in detail. It is found that using three smoothing cells for bending strain energy integration and one smoothing cell for shear strain energy integration achieve most accurate results and hence these numbers recommended for plates and shells in this study. In the geometrically nonlinear analysis, the total Lagrangian approach is adopted. The arc-length technique in conjunction with the modified Newton-Raphson method is utilized to solve the nonlinear equations. The numerical examples demonstrate that the present SFEM provides very stable and most accurate results with the similar computational effort compared to the existing FEM techniques tested in this work.

Keyword: smoothed finite element method, plate and shell, mid-rectangle rule, nonlinear, smoothed weak form.

[1] State Key Laboratory of Advanced Design and Manufacturing for Vehicle Body, Hunan University, Changsha, 410082, PR China.

[2] Centre for Advanced Computations in Engineering Science (ACES), Department of Mechanical Engineering, National University of Singapore, 9 Engineering Drive 1, 117576 Singapore.

[3] Singapore-MIT Alliance (SMA), E4-04-10, 4 Engineering Drive 3, 117576, Singapore

1 Introduction

In the past decades, the finite element method (FEM) has been playing a very important role in solving various problems in engineering and science, including mechanics problems of plates and shells [Zienkiewicz and Taylor (2000); Liu and Quek (2003)]. A number of plate and shell elements have been developed for linear and nonlinear analysis. Batoz and Tahar (1982) proposed a discrete Kirchhoff quadrilateral element (DKQ), which can give efficient results for bending problems for thin plates, but not for thick plates. Bathe and Dvorkin (1985) presented a 4-node plate element based on Mindlin-Reissner theory using mixed interpolated tensorial components (MITC). Belytschko and Leviathan (1994) developed a one point quadrature quadrilateral shell element with physical hourglass control. In recent years, meshfree methods have been developed and achieved remarkable progress for solving plate and shell problems, and many works are summarized in the book by Liu (2002), Atluri (2005). Chen and Liu (2001) had used the element free Galerkin (EFG) method for solving static and dynamic problem of thin plate of complicated shape. Composite laminated plates had also been studied for vibration problems, buckling problems [Chen et al. (2002, 2003)]. Shells had also been analyzed using EFG [Liu et al. (2002)]. Wang and Chen (2004) presented a Mindlin-Reissner plate formulation using a stabilized conforming nodal integration to mitigate the shear locking. A radial point interpolation method [Liu et al. (2008)] was formulated for plate problems using the smoothed nodal integration. Meshless Local Petrov-Galerkin (MLPG) Method [Atluri and Shen (2002); Atluri (2004)] was also employed for plates and shells analysis by many researchers [Gu and Liu (2001); Long

and Atluri (2002); Soric et al. (2004); Li et al. (2005); Sladek et al. (2006); Jarak et al. (2007)], and Atluri et al. (2004) proposed a meshless finite volume method through the MLPG "mixed" approach. For nonlinear analysis of plates and shells, Horrigmoe and Bergan (1978) presented a general formulation for geometrically nonlinear analysis of shells using flat finite elements. Hughes and Liu (1981) presented a general nonlinear finite element formulation using uniform reduced integration for shell analysis. Recently, Lee et al. (2002) introduced a geometrically nonlinear assumed strain formulation of a nine-node solid shell element. Wen and Hon (2007) formulated a Reissner-Mindlin plate element for geometrically nonlinear analysis by using a meshless collocation method. The other works of plates and shells analysis include those given by Basar and Kintzell (2003), Qian et al. (2003), Suetake (2006).

Although a significant mount of works have been done using FEM, some inherent problems related to element distortion still remain unsolved. Liu et al. (2007a) proposed a smoothed finite element method (SFEM) by combining the standard FEM with the strain smoothing technique used in meshfree methods [Chen et al. (2005)]. The SFEM further divides the elements into smoothing cells and computes the integrals along the edges of the smoothing cells based on the Green's divergence theorem. The n-sided polygonal element can be easily carried out using the SFEM [Dai et al. (2007)]. Liu et al. (2007b) gave detailed theoretical aspects including stability, bound property and convergence about the SFEM and revealed a number of attractive features resulted from the "softening" effects of the strain smoothing technique. Other problems solved using SFEM including free and forced vibration analysis [Dai and Liu (2007)], piezoelectric element analysis of two-dimensional smart structures [Nguyen-Van et al. (2008)]. A plate element [Nguyen-Xuan et al. (2008)] has been formulated using the SFEM. In Nguyen-Xuan's work, only linear plate problem is considered and the formulation is the combination of SFEM and MITC, in which only the bending term is formulated by using SFEM, and shear term is same as MITC element.

In the present paper, the smoothed finite element method (SFEM) is further extended to linear and geometrically nonlinear analysis of plates and shells. In the present work, all terms of the element are formulated by using the SFEM, and we overcome the shear locking by using fewer smoothing cells in shear term than those in membrane and bending terms. The smoothed strains are computed directly only using shape functions, and the shape functions of arbitrary point in the quadrilateral element are created in a trivial, simple and explicit manner. Through an intensive numerical study, it is found that three smoothing cells for bending strain energy integration, and one cell for shear strain energy integration in an element produces the most accurate solutions that are much more accurate compared with the existing FEM techniques.

2 Basic formulation

2.1 Kinematics of shells

In this section, the basic equations of shell theory are briefed. Based on the first order shear deformation theory, the displacements $\mathbf{u} = [u, v, w]$ at a local coordinate system (x, y, z) are expressed as follows:

$$\begin{aligned} u(x,y,z) &= u_0(x,y) - z\theta_x(x,y) \\ v(x,y,z) &= v_0(x,y) - z\theta_y(x,y) \\ w(x,y,z) &= w_0(x,y) \end{aligned} \tag{1}$$

where u_0, v_0 and w_0 are the displacements of the mid-plane of the shell in the x, y and z directions, θ_x and θ_y denote the rotations about the y and x axes, respectively, as shown in Fig. 1.

The strain vector $\boldsymbol{\varepsilon}$ can be written in terms of the mid-plane deformations using Eq. (1), which gives:

$$\boldsymbol{\varepsilon} = \begin{Bmatrix} \varepsilon_{xx} \\ \varepsilon_{yy} \\ \varepsilon_{xy} \\ \varepsilon_{xz} \\ \varepsilon_{yz} \end{Bmatrix} = \begin{Bmatrix} \boldsymbol{\varepsilon}_m \\ 0 \end{Bmatrix} + \begin{Bmatrix} z\boldsymbol{\varepsilon}_b \\ 0 \end{Bmatrix} + \begin{Bmatrix} 0 \\ \boldsymbol{\varepsilon}_s \end{Bmatrix} \tag{2}$$

where $\boldsymbol{\varepsilon}_m$ is the membrane strain, $\boldsymbol{\varepsilon}_b$ is the bending strain, and $\boldsymbol{\varepsilon}_s$ is the shear strain. Bending and

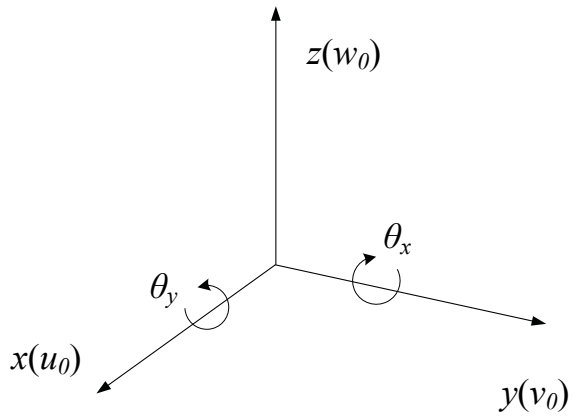

Figure 1: Local coordinate system with the x-y plane siting on the shell mid-plane

shear strains can be written as:

$$\boldsymbol{\varepsilon}_b = -\begin{Bmatrix} \frac{\partial \theta_x}{x} \\ \frac{\partial \theta_y}{y} \\ \frac{\partial \theta_x}{y} + \frac{\partial \theta_y}{x} \end{Bmatrix}, \quad \boldsymbol{\varepsilon}_s = \begin{Bmatrix} \frac{\partial w_0}{x} - \theta_x \\ \frac{\partial w_0}{y} - \theta_y \end{Bmatrix} \tag{3}$$

For nonlinear analysis, the membrane strain is given by:

$$\boldsymbol{\varepsilon}_m = \begin{Bmatrix} \frac{\partial u_0}{x} + \frac{1}{2}\left(\frac{\partial w}{x}\right)^2 \\ \frac{\partial v_0}{y} + \frac{1}{2}\left(\frac{\partial w}{y}\right)^2 \\ \frac{\partial u_0}{y} + \frac{\partial v_0}{x} + \frac{\partial w}{x}\frac{\partial w}{y} \end{Bmatrix} = \boldsymbol{\varepsilon}_m^0 + \boldsymbol{\varepsilon}_m^{nl} \tag{4}$$

in which

$$\boldsymbol{\varepsilon}_m^0 = \begin{Bmatrix} \frac{\partial u_0}{x} \\ \frac{\partial v_0}{y} \\ \frac{\partial u_0}{y} + \frac{\partial v_0}{x} \end{Bmatrix}, \quad \boldsymbol{\varepsilon}_m^{nl} = \begin{Bmatrix} \frac{1}{2}\left(\frac{\partial w}{x}\right)^2 \\ \frac{1}{2}\left(\frac{\partial w}{y}\right)^2 \\ \frac{\partial w}{x}\frac{\partial w}{y} \end{Bmatrix} \tag{5}$$

and for linear analysis,

$$\boldsymbol{\varepsilon}_m = \boldsymbol{\varepsilon}_m^0 \tag{6}$$

Using Eq. (2), the generalized strain vector $\hat{\boldsymbol{\varepsilon}}$ can be written as:

$$\hat{\boldsymbol{\varepsilon}} = \begin{Bmatrix} \boldsymbol{\varepsilon}_m \\ \boldsymbol{\varepsilon}_b \\ \boldsymbol{\varepsilon}_s \end{Bmatrix} \tag{7}$$

The constitutive relationship can be expressed as:

$$\hat{\boldsymbol{\sigma}} = \hat{\mathbf{D}}\hat{\varepsilon} \tag{8}$$

where

$$\hat{\boldsymbol{\sigma}} = \begin{bmatrix} \hat{\mathbf{N}} \\ \hat{\mathbf{M}} \\ \hat{\mathbf{Q}} \end{bmatrix}, \quad \hat{\mathbf{D}} = \begin{bmatrix} \mathbf{D}_m & \mathbf{0} & \mathbf{0} \\ \mathbf{0} & \mathbf{D}_b & \mathbf{0} \\ \mathbf{0} & \mathbf{0} & \mathbf{D}_s \end{bmatrix} \tag{9}$$

in which $\hat{\mathbf{N}} = \begin{Bmatrix} N_x & N_y & N_{xy} \end{Bmatrix}^{\mathrm{T}}$ is the membrane force vector in the mid-plane, $\hat{\mathbf{M}} = \begin{Bmatrix} M_x & M_y & M_{xy} \end{Bmatrix}^{\mathrm{T}}$ is the bending moment vector, $\hat{\mathbf{Q}} = \begin{Bmatrix} Q_x & Q_y \end{Bmatrix}^{\mathrm{T}}$ is the transverse shear force vector, $\mathbf{D}_m$ is the membrane stiffness constitutive coefficients, $\mathbf{D}_b$ is the bending stiffness constitutive coefficients, and $\mathbf{D}_s$ is the transverse shear stiffness constitutive coefficients:

$$\mathbf{D}_m = \int_{-\frac{t}{2}}^{\frac{t}{2}} \mathbf{D}_0 \mathrm{d}z = t\mathbf{D}_0 \tag{10}$$

$$\mathbf{D}_b = \int_{-\frac{t}{2}}^{\frac{t}{2}} z^2 \mathbf{D}_0 \mathrm{d}z = \frac{t^3}{12}\mathbf{D}_0 \tag{11}$$

$$\mathbf{D}_s = \int_{-\frac{t}{2}}^{\frac{t}{2}} kG \begin{bmatrix} 1 & 0 \\ 0 & 1 \end{bmatrix} \mathrm{d}z = \kappa t G \begin{bmatrix} 1 & 0 \\ 0 & 1 \end{bmatrix} \tag{12}$$

where t is the thickness of the plate or shell, G is shear modulus, $\kappa = 5/6$ is the shear correction factor, and $\mathbf{D}_0$ is the constitutive coefficients matrix given as:

$$\mathbf{D}_0 = \frac{E}{1-\nu^2}\begin{bmatrix} 1 & \nu & 0 \\ \nu & 1 & 0 \\ 0 & 0 & (1-\nu)/2 \end{bmatrix} \tag{13}$$

where E is Young's modulus and ν is Poisson's ratio.

From Eq. (1), the generalized mid-plane displacements vector $\hat{\mathbf{u}}$ is defined as:

$$\hat{\mathbf{u}} = \begin{Bmatrix} u_0 & v_0 & w_0 & \theta_x & \theta_y \end{Bmatrix}^{\mathrm{T}} \tag{14}$$

The displacements at any point in an element are interpolated using the nodal displacements at the nodes using the element shape functions created by the element nodes. Both displacements and rotations use the same shape functions. The bilinear quadrilateral elements are used here, and the generalized mid-plane displacement vector $\hat{\mathbf{u}}$ can be then expressed as:

$$\hat{\mathbf{u}}(\mathbf{x}) = \sum_{I=1}^{4} \mathbf{N}_I(\mathbf{x})\,\mathbf{d}_I \tag{15}$$

where $\mathbf{d}_I = \{u_I, v_I, w_I, \theta_{xI}, \theta_{yI}\}^{\mathrm{T}}$ is the nodal displacement at node I, and the diagonal matrix of shape functions

$$\mathbf{N}_I(\mathbf{x}) = \begin{bmatrix} N_I(\mathbf{x}) & 0 & 0 & 0 & 0 \\ 0 & N_I(\mathbf{x}) & 0 & 0 & 0 \\ 0 & 0 & N_I(\mathbf{x}) & 0 & 0 \\ 0 & 0 & 0 & N_I(\mathbf{x}) & 0 \\ 0 & 0 & 0 & 0 & N_I(\mathbf{x}) \end{bmatrix} \tag{16}$$

in which $N_I(\mathbf{x})$ is the shape function associated to node I.

2.2 Smoothing cells in SFEM

As shown in Fig. 2, the problem domain Ω is divided into N_e quadrilateral elements, as in the standard FEM. The quadrilateral element Ω_k is further divided into SC smoothing cells, $\Omega_{k1}, \Omega_{k2}, \ldots, \Omega_{k\mathrm{SC}}$, such that $\Omega_k = \Omega_{k1} \cup \Omega_{k2} \cup \ldots \cup \Omega_{k\mathrm{SC}}$ and $\Omega_{ki} \cap \Omega_{kj} = \emptyset$, $(i \neq j,\ i = 1, \ldots, \mathrm{SC},\ j = 1, \ldots, \mathrm{SC})$. In the present SFEM, we use the strain smoothing operation for each of the cells:

$$\overline{\boldsymbol{\varepsilon}}^0_{mi} = \frac{1}{A_{ki}} \int_{\Omega_{ki}} \boldsymbol{\varepsilon}^0_m(\mathbf{x}) \mathrm{d}\Omega \tag{17a}$$

$$\overline{\boldsymbol{\varepsilon}}_{bi} = \frac{1}{A_{ki}} \int_{\Omega_{ki}} \boldsymbol{\varepsilon}_b(\mathbf{x}) \mathrm{d}\Omega \tag{17b}$$

$$\overline{\boldsymbol{\varepsilon}}_{si} = \frac{1}{A_{ki}} \int_{\Omega_{ki}} \boldsymbol{\varepsilon}_s(\mathbf{x}) \mathrm{d}\Omega \tag{17c}$$

$$\overline{\boldsymbol{\varepsilon}}^{nl}_{mi} = \frac{1}{A_{ki}} \int_{\Omega_{ki}} \boldsymbol{\varepsilon}^{nl}_m(\mathbf{x}) \mathrm{d}\Omega \tag{17d}$$

where $\overline{\boldsymbol{\varepsilon}}^0_{mi}$, $\overline{\boldsymbol{\varepsilon}}_{bi}$, $\overline{\boldsymbol{\varepsilon}}_{si}$ and $\overline{\boldsymbol{\varepsilon}}^{nl}_{mi}$ are the averaged/smoothed strains, and A_{ki} is the area of the ith cell Ω_{ki} of the kth element.

2.3 Integration scheme with strain smoothing operation

Consider an element of the problem domain, substituting Eqs. (5) and (16) into Eq. (17a), the smoothed strains $\overline{\boldsymbol{\varepsilon}}^0_{mi}$ can also be written in matrix form of:

$$\begin{aligned} \overline{\boldsymbol{\varepsilon}}^0_{mi} &= \frac{1}{A_{ki}} \int_{\Gamma_{ki}} \mathbf{n}\hat{\mathbf{u}}(\mathbf{x}) d\Gamma = \sum_{I=1}^{4} \mathbf{n}\mathbf{N}_I(\mathbf{x}) \mathbf{d}_I \\ &= \sum_{I=1}^{4} \left(\hat{\mathbf{B}}^0_{mi}\right)_I \mathbf{d}_I \end{aligned} \tag{18}$$

where $\mathbf{n}$ is is the outward normal matrix containing the components of the outward normal vector to boundary Γ_{ki}, and $\hat{\mathbf{B}}^0_{mi}$ is the smoothed linear membrane strain matrix given by:

$$\left(\hat{\mathbf{B}}^0_{mi}\right)_I = \begin{bmatrix} \overline{b}_{iIx} & 0 & 0 & 0 & 0 \\ 0 & \overline{b}_{iIy} & 0 & 0 & 0 \\ \overline{b}_{iIy} & \overline{b}_{iIx} & 0 & 0 & 0 \end{bmatrix} \tag{19}$$

in which

$$\begin{aligned} \overline{b}_{iIx} &= \frac{1}{A_{ki}} \int_{\Gamma_{ki}} n_x \cdot N_I(\mathbf{x}) d\Gamma \\ &= \frac{1}{A_k} \sum_{j=1}^{Nl} n_{xj} \cdot N_I(\mathbf{x}_{ngj}) \cdot l_j \end{aligned} \tag{20a}$$

$$\begin{aligned} \overline{b}_{iIy} &= \frac{1}{A_{ki}} \int_{\Gamma_{ki}} n_y \cdot N_I(\mathbf{x}) d\Gamma \\ &= \frac{1}{A_k} \sum_{j=1}^{Nl} n_{yj} \cdot N_I(\mathbf{x}_{ngj}) \cdot l_j \end{aligned} \tag{20b}$$

In Eq. (20), Nl is the total number of the segments of Γ_{ki}, n_{xj} and n_{yj} are the components of the outward unit normal to the jth boundary segment, $\mathbf{x}_{ngj}$ is the coordinate value of Gauss point of the jth boundary segment. The shape function of local point in the element is shown in Fig.3.

Similarly, the smoothed bending strain over the domain Ω_{ki} can be rewritten as

$$\overline{\boldsymbol{\varepsilon}}_{bi} = \sum_{I=1}^{4} \left(\hat{\mathbf{B}}_{bi}\right)_I \mathbf{d}_I \tag{21}$$

where $\hat{\mathbf{B}}_{bi}$ is the smoothed bending strain matrix of the domain Ω_{ki} given by

$$\left(\hat{\mathbf{B}}_{bi}\right)_I = \begin{bmatrix} 0 & 0 & 0 & -\overline{b}_{iIx} & 0 \\ 0 & 0 & 0 & 0 & -\overline{b}_{iIy} \\ 0 & 0 & 0 & -\overline{b}_{iIy} & -\overline{b}_{iIx} \end{bmatrix} \tag{22}$$

The smoothed shear strain over the domain Ω_{ki} can be expressed as

$$\overline{\boldsymbol{\varepsilon}}_{si} = \sum_{I=1}^{4} \left(\hat{\mathbf{B}}_{si}\right)_I \mathbf{d}_I \tag{23}$$

in which

$$\left(\hat{\mathbf{B}}_{si}\right)_I = \begin{bmatrix} 0 & 0 & \overline{b}_{iIx} & -sh_I & 0 \\ 0 & 0 & \overline{b}_{iIy} & 0 & -sh_I \end{bmatrix} \tag{24}$$

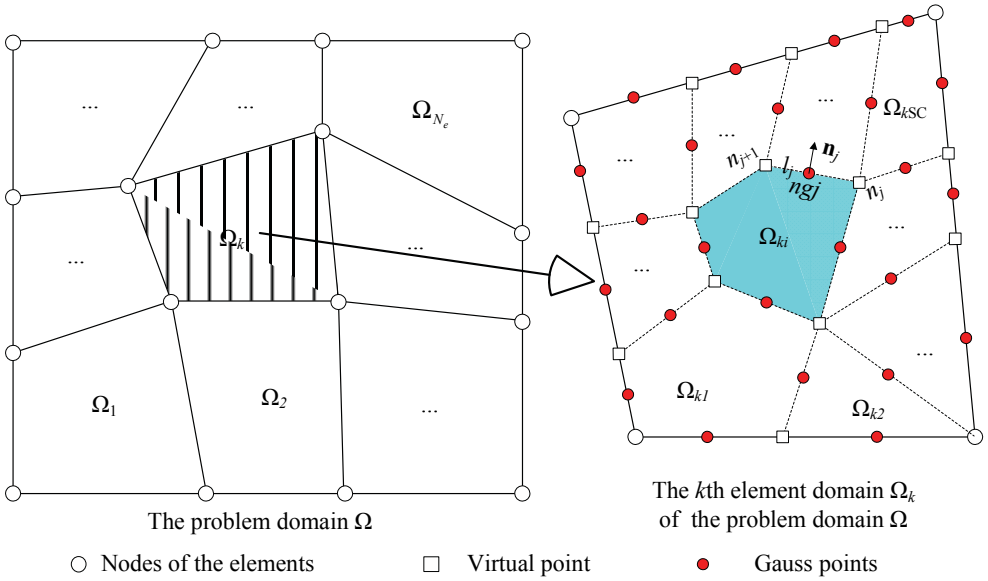

Figure 2: The problem domain Ω is divided into N_e quadrilateral elements, the kth element of domain Ω_k is further divided into SC smoothing cells.

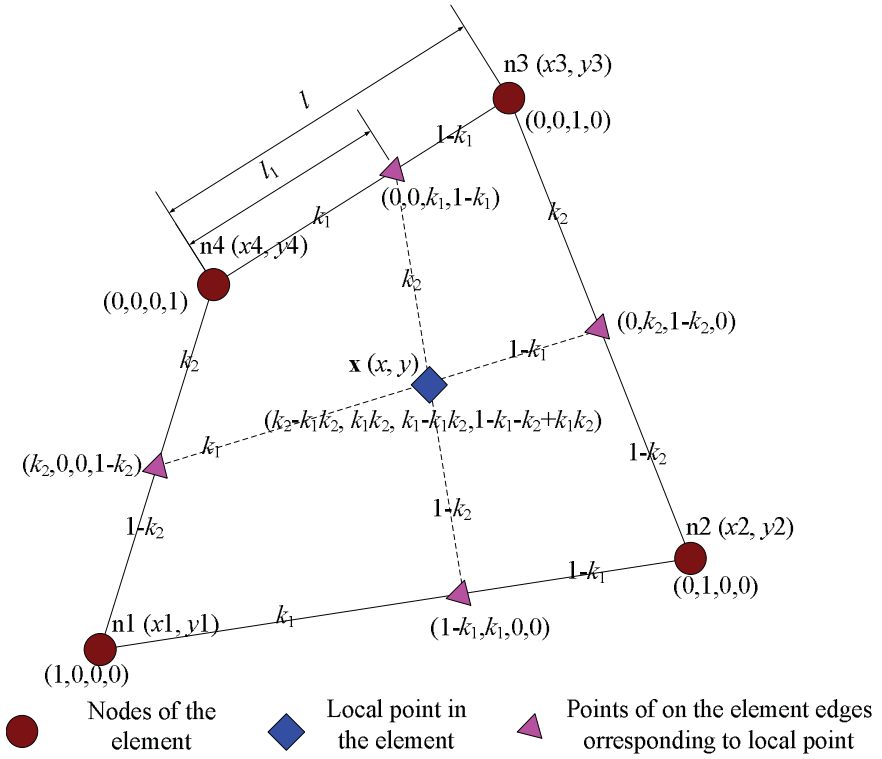

Figure 3: The shape function of local point in the element. $k_1 = l_1/l$ is a proportion, and k_2 has the same meaning.

In Eq. (24), sh_I can be defined by

$$sh_I = \frac{1}{N_n}\sum_{j=1}^{N_n} N_I(\mathbf{x}_j) \tag{25}$$

where N_n is the total number of the nodes of the smoothing cell Ω_{ki}, and $N_I(\mathbf{x}_j)$ is the shape function value of the jth node of the cell Ω_{ki}.

Using Eqs. (5), (15) and (17d), we obtain the smoothed nonlinear strain over the domain Ω_{ki} as follows

$$\overline{\boldsymbol{\varepsilon}}_{mi}^{nl} = \sum_{I=1}^{4}\left(\frac{1}{2}\hat{\mathbf{B}}_{mi}^{nl}\right)_I \mathbf{d}_I \tag{26}$$

$\hat{\mathbf{B}}_{mi}^{nl}$ is the smoothing nonlinear strain matrix in the smoothing cell given by

$$\left(\hat{\mathbf{B}}_{mi}^{nl}\right)_I = \mathbf{A}(\mathbf{G}_i)_I \tag{27}$$

in which

$$(\mathbf{G}_i)_I = \begin{bmatrix} 0 & 0 & \overline{b}_{iIx} & 0 & 0 \\ 0 & 0 & \overline{b}_{iIy} & 0 & 0 \end{bmatrix} \tag{28}$$

$$\mathbf{A} = \sum_{I=1}^{4}\begin{bmatrix} \overline{b}_{iIx}w_I & 0 & \overline{b}_{iIx}w_I \\ 0 & \overline{b}_{iIx}w_I & \overline{b}_{iIx}w_I \end{bmatrix}^{\mathrm{T}} \tag{29}$$

where w_I is the deflection at the node I of the element.

Using Eqs. (6), (18), (21), (23) and (26), the smoothing generalized strain $\overline{\hat{\boldsymbol{\varepsilon}}}$ in each cell can be written as:

$$\overline{\hat{\boldsymbol{\varepsilon}}}_i = \sum_{I=1}^{4}\left(\left(\hat{\mathbf{B}}_i^0\right)_I + \frac{1}{2}\left(\hat{\mathbf{B}}_i^{nl}\right)_I\right)\mathbf{d}_I \tag{30}$$

where $\hat{\mathbf{B}}_i^0$ is the smoothing linear strain matrix, and $\hat{\mathbf{B}}_i^{nl}$ is the smoothing nonlinear strain matrix given by:

$$\hat{\mathbf{B}}_i^0 = \begin{bmatrix} \hat{\mathbf{B}}_{mi}^0 \\ \hat{\mathbf{B}}_{bi} \\ \hat{\mathbf{B}}_{si} \end{bmatrix}, \quad \hat{\mathbf{B}}_i^{nl} = \begin{bmatrix} \hat{\mathbf{B}}_{mi}^{nl} \\ \mathbf{0} \\ \mathbf{0} \end{bmatrix} \tag{31}$$

3 Discrete equations

3.1 Smoothed Galerkin weak form

In the present SFEM, the displacement solution $\hat{\mathbf{u}}$ and the corresponding smoothed strain $\overline{\hat{\boldsymbol{\varepsilon}}}$ obtained using $\hat{\mathbf{u}}$ satisfy the following smoothed Galerkin weak form:

$$\int_\Omega \delta\overline{\hat{\boldsymbol{\varepsilon}}}^{\mathrm{T}}\hat{\mathbf{D}}\overline{\hat{\varepsilon}}\mathrm{d}\Omega - \int_\Omega \delta\hat{\mathbf{u}}^{\mathrm{T}}\tilde{\mathbf{f}}\mathrm{d}\Omega = 0 \tag{32}$$

where $\tilde{\mathbf{f}}$ represents the external load applied over the problem domain Ω. The properties of the smoothed Galerkin weak form are examined and proven by Liu (2008).

Substituting Eq. (15) into Eq. (32) and using the strain-displacement relation, a set of discretized algebraic system equations can be obtained in the following matrix form:

$$\overline{\mathbf{K}}\mathbf{d} - \mathbf{f} = 0 \tag{33}$$

where $\overline{\mathbf{K}}$ is the *smoothed* stiffness matrix, and $\mathbf{f}$ is the force vector defined as:

$$\mathbf{f} = \int_\Omega \mathbf{N}(\mathbf{x})\tilde{\mathbf{f}}d\Omega \tag{34}$$

In obtaining the *smoothed* stiffness $\overline{\mathbf{K}}$, the integrations over the problem domain Ω need to be performed based on each element. In each element, the smoothed strains introduced in last section are used and the *smoothed* stiffness is given by:

$$\overline{\mathbf{K}}_{IJ} = \sum_{i=1}^{\mathrm{SC}}\int_{\Omega_i}\left(\hat{\mathbf{B}}_i\right)_I^{\mathrm{T}}\hat{\mathbf{D}}\left(\hat{\mathbf{B}}_i^0 + \frac{1}{2}\hat{\mathbf{B}}_i^{nl}\right)_J d\Omega \tag{35}$$

where $\hat{\mathbf{B}}_i$ is strain matrix, it is given as:

$$\hat{\mathbf{B}}_i = \hat{\mathbf{B}}_i^0 + \hat{\mathbf{B}}_i^{nl} = \begin{bmatrix} \hat{\mathbf{B}}_{mi}^0 \\ \hat{\mathbf{B}}_{bi} \\ \hat{\mathbf{B}}_{si} \end{bmatrix} + \begin{bmatrix} \hat{\mathbf{B}}_{mi}^{nl} \\ \mathbf{0} \\ \mathbf{0} \end{bmatrix} \tag{36}$$

Substituting Eq. (36) into Eq. (35), the stiffness matrix can be written as:

$$\overline{\mathbf{K}}_{IJ} = \overline{\mathbf{K}}_{IJ}^0 + \overline{\mathbf{K}}_{IJ}^{nl} \tag{37}$$

For linear analysis

$$\overline{\mathbf{K}}_{IJ} = \overline{\mathbf{K}}_{IJ}^0 \tag{38}$$

The matrices $\overline{\mathbf{K}}_{IJ}^0$ and $\overline{\mathbf{K}}_{IJ}^{nl}$ are given as:

$$\begin{aligned}\overline{\mathbf{K}}_{IJ}^0 &= \sum_{i=1}^{\mathrm{SC}}\left(\hat{\mathbf{B}}_i^0\right)_I^{\mathrm{T}}\hat{\mathbf{D}}\left(\hat{\mathbf{B}}_i^0\right)_J A_i \\ &= \overline{\mathbf{K}}_{IJ}^m + \overline{\mathbf{K}}_{IJ}^b + \overline{\mathbf{K}}_{IJ}^s\end{aligned} \tag{39}$$

$$\overline{\mathbf{K}}_{IJ}^{m} = \sum_{i=1}^{\mathrm{SC1}} \left(\hat{\mathbf{B}}_{mi}^{0}\right)_I^{\mathrm{T}} \mathbf{D}_m \left(\hat{\mathbf{B}}_{mi}^{0}\right)_J A_i \tag{40}$$

$$\overline{\mathbf{K}}_{IJ}^{b} = \sum_{i=1}^{\mathrm{SC2}} \left(\hat{\mathbf{B}}_{bi}\right)_I^{\mathrm{T}} \mathbf{D}_b \left(\hat{\mathbf{B}}_{bi}\right)_J A_i \tag{41}$$

$$\overline{\mathbf{K}}_{IJ}^{s} = \sum_{i=1}^{\mathrm{SC3}} \left(\hat{\mathbf{B}}_{si}\right)_I^{\mathrm{T}} \mathbf{D}_s \left(\hat{\mathbf{B}}_{si}\right)_J A_i \tag{42}$$

$$\overline{\mathbf{K}}_{IJ}^{nl} = \sum_{i=1}^{\mathrm{SC4}} \begin{pmatrix} \frac{1}{2}\left(\hat{\mathbf{B}}_i^{0}\right)_I^{\mathrm{T}} \hat{\mathbf{D}} \left(\hat{\mathbf{B}}_i^{nl}\right)_J \\ +\left(\hat{\mathbf{B}}_i^{nl}\right)_I^{\mathrm{T}} \hat{\mathbf{D}} \left(\hat{\mathbf{B}}_i^{0}\right)_J \\ +\frac{1}{2}\left(\hat{\mathbf{B}}_i^{nl}\right)_I^{\mathrm{T}} \hat{\mathbf{D}} \left(\hat{\mathbf{B}}_i^{nl}\right)_J \end{pmatrix} A_i \tag{43}$$

where A_i is the area of the ith smoothing cell, and SC1, SC2, SC3 and SC4 are the smoothing cell numbers and which can be given different values.

Note: For present method, we first use the same set of bilinear shape functions as standard FEM; therefore, the assumed displacement $\mathbf{u}$ and the force vector $\mathbf{f}$ in present method are the same to standard FEM. Only the smoothed strains $\bar{\hat{\boldsymbol{\varepsilon}}}$ in present method and the resultant strains $\hat{\boldsymbol{\varepsilon}}$ in standard FEM are different, and so are the solutions of the nodal displacements$\mathbf{d}$.

3.2 Formulation for nonlinear problems

The Modify Newton-Raphson method is empolyed here to solve the assembled nonlinear equilibrium equations. An incremental form of Eq. (33), required by the Newton-Raphson method, should be provided. It is can be rearranged as:

$$\mathbf{g}(\mathbf{d}) = \overline{\mathbf{K}}\mathbf{d} - \mathbf{F} = 0 \tag{44}$$

The external load $\mathbf{F}$ is assumed to be proportional to the fixed load $\mathbf{F}_0$ as:

$$\mathbf{F} = \lambda \mathbf{F}_0 \tag{45}$$

where λ is the load level parameter. The nonlinear equilibrium equation (44) can be rewritten as:

$$\mathbf{g}(\mathbf{d}, \lambda) = \overline{\mathbf{K}}\mathbf{d} - \lambda \mathbf{F}_0 \tag{46}$$

In order to arrive at a new equilibrium state, displacement and load level parameter are updated by increments. The following incremental form of the equation can be attained via a truncated Taylor series expansion,

$$\mathbf{g}(\mathbf{d} + \Delta\mathbf{d}, \lambda + \Delta\lambda) = \mathbf{g}(\mathbf{d}, \lambda) + \overline{\mathbf{K}}^{t} \Delta\mathbf{d} - \Delta\lambda \mathbf{F}_0 = 0 \tag{47}$$

where $\Delta\mathbf{d}$ and $\Delta\lambda$ are the displacement increment and load increment factors, respectively. $\overline{\mathbf{K}}^{t}$ is the *smoothed* tangent stiffness matrix which is given by:

$$\overline{\mathbf{K}}_{IJ}^{t} = \sum_{i=1}^{\mathrm{SC}} \left(\hat{\mathbf{B}}_i\right)_I^{\mathrm{T}} \hat{\mathbf{D}} \left(\hat{\mathbf{B}}_i\right)_J A_i + \sum_{i=1}^{\mathrm{SC}} \left(\mathbf{G}_i\right)_I^{\mathrm{T}} \check{\mathbf{N}} \left(\mathbf{G}_i\right)_J A_i \tag{48}$$

where $\hat{\mathbf{B}}_i$ is given in Eq. (36), $\mathbf{G}_i$ is given in Eq. (28), $\check{\mathbf{N}}$ is the membrane stress matrix given as:

$$\check{\mathbf{N}} = \begin{bmatrix} N_{xx} & N_{xy} \\ N_{xy} & N_{yy} \end{bmatrix} \tag{49}$$

where N_{xx}, N_{xy}, N_{yy} are the components of membrane force $\hat{\mathbf{N}}$ given in Eq. (9).

In the incremental-iterative method, each load step includes the application of external load and subsequent iterations to restore equilibrium. In subsequent iterations, the displacement increment is written as:

$$\begin{aligned} \Delta\mathbf{d}_n^{j+1} &= \left[\left(\overline{\mathbf{K}}^{t}\right)_n\right]^{-1} \left(\Delta\lambda_n^{j+1}\mathbf{F}_0 - \mathbf{g}_n^{j}\right) \\ &= \left[\left(\overline{\mathbf{K}}^{t}\right)_n\right]^{-1} \\ &\quad \left\{\Delta\lambda_n^{j+1}\mathbf{F}_0 - \left[\overline{\mathbf{K}}\left(\mathbf{d}_n^{j}\right)\mathbf{d}_n - \lambda_n^{j}\mathbf{F}_0\right]\right\} \end{aligned} \tag{50}$$

where the subscript n is used to denote the load step number and the subscript j is used to represent the subsequent iteration cycle. The Arc-length method presented by Crisfield (1997) is used to overcome the 'snap-throughs' and the 'snap-backs'. The convergence is checked using following criterion:

$$\frac{\|\mathbf{g}(\mathbf{d}, \lambda)\|}{\|\mathbf{F}(\mathbf{d}, \lambda)\|} < \delta \tag{51}$$

where δ is the tolerance for convergence constant which is set to 0.0001 in this study.

4 Numerical examples

4.1 Analysis of a square plate

In order to test the efficiency of the present SFEM, a square plate of the length L and the thickness t subjected to different boundary conditions is considered in this section. The material properties are taken as Young's modulus $E$and Poisson ratio υ. Owing to the symmetry of the problem, only a quarter of the plate is modeled, as shown in Fig.4.

4.1.1 Effect of the number of smoothing cells

A plate with L=10m and t=0.1m simply supported at all sides subjected to a transverse uniform load is investigated to study the effect of the number of smoothing cells used in the elements. The material properties are taken as Young's modulus $E = 3.0e7N/\text{m}^2$, Poisson ratio υ=0.3.

This problem is analyzed using different number of elements and smoothing cells as shown in Fig.5. In order to mitigate the shear locking effect, only one smoothing cell is used on the shear strain term, and six different divisions, SC=1, 2, 3, 4, 8 and 16, are used on the other terms. This technique to suppress the shear locking is the same as the reduced and selective integration techniques in FEM. For a comparison, the FEM quadrilateral element with reduced integration (Q4-R) proposed by Malkus and Hughes (1978) is also used in the analysis. The analytic solutions are given by Reismann (1988).

Table 1 shows the numerical results of central deflection and Fig. 6 shows the relative error between numerical results and analytical solutions of the problem using SFEM with different divisions of smoothing cells. From the result, it is seen that when the number of smoothing cells is one or two, numerical results are bigger than analytical solutions, and when the number of smoothing cells is three or more, the numerical results are smaller than analytical solutions. The more the smoothing cells, the smaller results obtained. Regardless of the numbers of the smoothing cells used, the SFEM is more accurate than the FEM quadrilateral element with reduced integration (Q4-R) for this problem. These findings confirm the properties of SFEM introduced

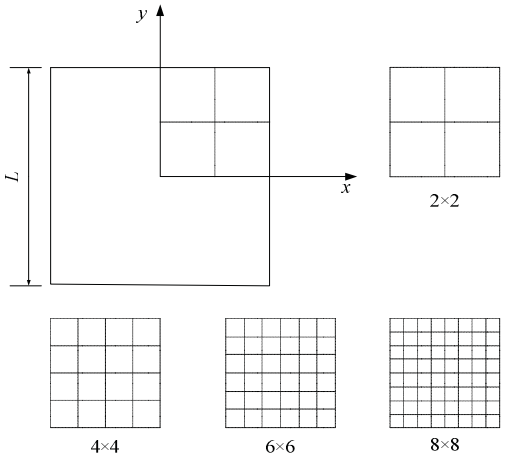

Figure 4: A quarter of a square plate is meshed with quadrilateral elements.

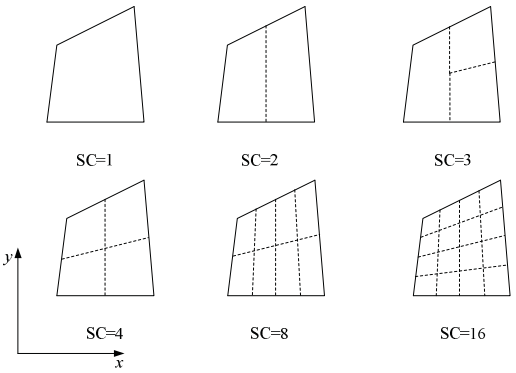

Figure 5: Division of an element into smoothing cells.

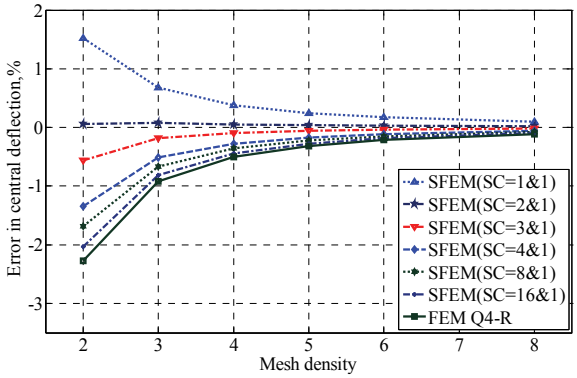

Figure 6: Comparison of central deflection computed using FEM and SFEM with different divisions of smoothing cells

]

Table 1: The central deflection $\hat{w}$ for a simply supported square plate with a uniform load computed using FEM and SFEM with different divisions of smoothing cells ($\hat{w} = w_c D/qL^4$).

Mesh	SC=1&1	SC=2&1	SC=3&1	SC=4&1	SC=8&1	SC=16&1	Q4-R
2×2	0.0041256	0.0040660	0.0040371	0.0040086	0.0039946	0.0039806	0.0039714
3×3	0.0040915	0.0040669	0.0040547	0.0040426	0.0040366	0.0040306	0.0040266
4×4	0.0040793	0.0040658	0.0040591	0.0040524	0.0040491	0.0040458	0.0040436
5×5	0.0040738	0.0040653	0.0040611	0.0040568	0.0040547	0.0040526	0.0040512
6×6	0.0040709	0.0040651	0.0040621	0.0040592	0.0040577	0.0040563	0.0040553
8×8	0.0040681	0.0040648	0.0040632	0.0040615	0.0040607	0.0040599	0.0040593
Analytic solution		0.004064					

by Liu et al. (2007b). There should be an optimal certain number of cells that can produce the most accurate result, and it is should be between 2∼4 for bilinear quadrilateral elements. Form the results of this problem, we find that SFEM with SC=3&1, meaning that three cells for bending and membrane terms and one for shearing term, gives the best results. Therefore, SFEM (SC=3&1) is used in plates and shells problems in the following section.

4.1.2 Shear locking

Shear locking results from the spurious appearance of transverse shear, which is generated due to the inability of the formulation based on the first order deformation theory in reproducing pure bending mode. In this work, we use only one smoothing cell in computing shear strain matrix for avoiding shear locking which is similar to one point quadrature used in the FEM. To study the effectiveness of the present SFEM, a simply supported uniformly loaded square plate is used in the examination.

For comparison, several existing FEM elements are also used in solving the same problem, including the mixed interpolated tensorial components element MITC4 [Bathe and Dvorkin (1985)], the reduced integration quadrilateral element Q4-R [Malkus and Hughes (1978)] and the discrete Kirchhoff quadrilateral element DKQ [Batoz and Tahar (1982)].

The results obtained using different methods are presented in Table 2 and Fig. 7 in terms of data and curves, respectively. It is clearly shown that the SFEM can give the most accurate solution for the full range of length/thickness ratio of the plate. It works for both thick and thin plates without shear lockings, even for extremely thin plate of length/thickness ratio $L/t = 10^7$.The DKQ was designed particularly for solving shear locking problems, and it indeed works well for thin plates. However, it gives wrong results for thick plates. MITC4 and Q4-R work well for thick plates, but the solution accuracy for the thin plates are much lower than SFEM (SC=3&1).

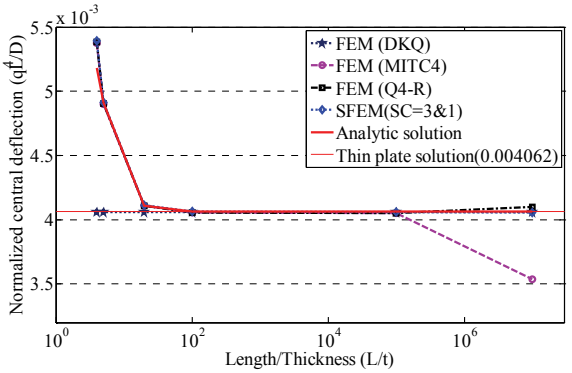

Figure 7: Shear locking test for a simply supported square plate.

4.1.3 Convergence and accuracy

In order to exam the convergence and accuracy of coarse meshes in thin and thick plate, the simply supported uniformly loaded square plate with various length ratios, a thin plate with L/t=100 and a thick plate with L/t=5 are investigated in this subsection. A set of five meshes are used for studying

Table 2: The central deflection $\hat{w}$ of a simply supported square plate subjected to a uniform load with different length/thickness ratios (mesh size:6×6, $\hat{w} = w_c D/qL^4$).

L/t	4	5	20	10^2	10^5	10^7
FEM (DKQ)	0.004061	0.004061	0.004061	0.004061	0.004061	0.004061
FEM (MITC4)	0.005376	0.004900	0.004106	0.004055	0.004053	0.003535
FEM (Q4-R)	0.005384	0.004905	0.004106	0.004055	0.004053	0.004101
SFEM(SC=3&1)	0.005390	0.004911	0.004113	0.004062	0.004060	0.004059
Analytic solution	0.005179	0.004907	0.004108	0.004064	0.004062	0.004062

Table 3: Numerical results of normalized central deflection $\hat{w}$ for a simply supported square plate subjected to uniform load ($L/t = 100$, $\hat{w} = w_c D/qL^4$).

Mesh	FEM (Q4-R)	FEM (DKQ)	FEM (MITC4)	SFEM (SC=3&1)
2×2	0.003971	0.004046	0.003971	0.004037
4×4	0.004044	0.004060	0.004044	0.004059
6×6	0.004055	0.004061	0.004055	0.004062
8×8	0.004059	0.004062	0.004059	0.004063
10×10	0.004061	0.004062	0.004061	0.004064
Analytic solution	0.004064			

Table 4: Numerical results of normalized central deflection $\hat{w}$ for a simply supported square plate subjected to uniform load ($L/t = 5$, $\hat{w} = w_c D/qL^4$).

Mesh	FEM (Q4-R)	FEM (DKQ)	FEM (MITC4)	SFEM (SC=3&1)
2×2	0.004921	0.004046	0.004855	0.004987
4×4	0.004906	0.004060	0.004894	0.004921
6×6	0.004905	0.004061	0.004900	0.004911
8×8	0.004904	0.004062	0.004902	0.004908
10×10	0.004904	0.004062	0.004903	0.004907
Analytic solution	0.004907			

here. Aforementioned existing quadrilateral plate elements which are introduced in last subsection are employed as comparison with present method.

Table 3 and Table 4 report the normalized central deflections of the thin plate and the thick plate. It is seen that the present SFEM has high accuracy at coarse meshes and fast convergence regardless of the thickness of the plate. DKQ works well for thin plates nevertheless it gives wrong results for thick plates. Both Q4-R and MITC4 have a slightly lower accuracy than SFEM (SC=3&1).

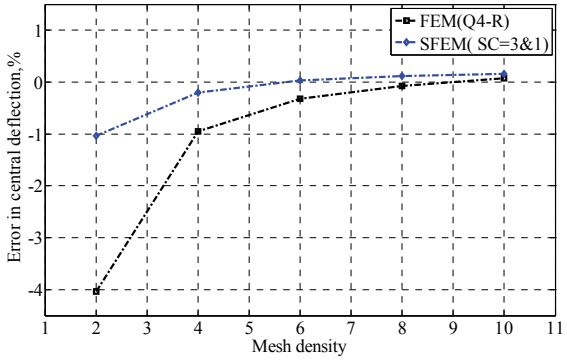

Figure 8: Relative error of the central deflection of the thin square plate with all sides clamped.

4.1.4 *Bending analysis with different boundary conditions*

A thin square plate with transverse uniform load subjected to different boundary conditions is analyzed in this subsection, length/thickness ratios L/t=100 is studied. All edges simply supported thin square plate has been investigated in last section, two boundary conditions are tested here: (a)

Table 5: The central deflection $\hat{w}$ for a square plate subjected to uniform load. (a) All sides clamped. (b) Two sides clamped and two sides simply supported ($L/t = 100$, $\hat{w} = w_c D/qL^4$).

Mesh	*a*		*b*	
	FEM (Q4-R)	SFEM(SC=3&1)	FEM (Q4-R)	SFEM(SC=3&1)
2×2	0.001214	0.001252	0.001737	0.001788
4×4	0.001253	0.001262	0.001879	0.001892
6×6	0.001261	0.001265	0.001902	0.001908
8×8	0.001264	0.001266	0.001910	0.001913
10×10	0.001266	0.001267	0.001914	0.001916
Analytic solution	0.001265		0.00192	

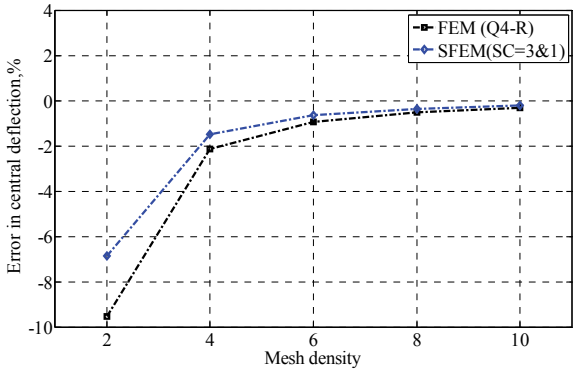

Figure 9: Relative error of the central deflection of the thin square plate with two sides clamped and two sides simply supported.

all edges clamped; (b) two edges clamped and two simply supported.

Table 5 shows a comparison of the present results with the numerical results obtained from FEM Quadrilateral element with reduced integration (Q4-R). The analytic solutions are given by Reismann (1988). The relative errors of the central deflection between numerical results and analytical solutions are shown in Fig. 8 and Fig. 9. It can be seen that for both boundary conditions, the solution of the present SFEM is more accurate than that of the FEM Q4-R element. The SFEM model is less stiff than that of FEM of Q4-R element, which confirms the properties of SFEM discussed in subsection 4.1.1.

4.1.5 Nonlinear analysis

In this subsection, a clamped square plate under uniformly distributed load q is analyzed for geometrically nonlinear behavior using SFEM (SC=3&1). The side length and thickness of the square plate are L=100mm and t=1mm. The material properties for this plate are E=2.1e06N/mm^2 and υ=0.316. The analytic solutions of central deflection are given by Chia (1980).

$$\left(\frac{w_{11}}{t}\right)^3 + 0.2522\frac{w_{11}}{t} = 0.0001333\frac{qL^4}{Dt} \qquad (52)$$
$$w_0 = 2.5223 w_{11}$$

where w_0 is the central deflection and D is the bending stiffness given as $D = Et^3/12\left(1-\nu^2\right)$.

A quarter of the plate is modeled due to the symmetry. The numerical solutions are obtained using four meshes of 2×2, 4×4, 6×6, 8×8. The nondimensional central deflection w_0/t is computed using the presented SFEM and listed in Table 6. Fig. 10 shows the load-displacement curves of numerical results computed from present method with different mesh density and analytic solutions calculated using Eq. (52). It is observed that the results converge very quickly to the analytic solution. When the mesh density is 8×8, the numerical results curve is very closed to analytic solutions curve.

4.2 Analysis of circular plate

Linear and nonlinear analysis of a clamped circular plate subjected to uniform load is further studied in this section. The configuration and mesh are shown in Fig. 11; the radius of the plate is R=5m and the thickness is t=0.1m. Poisson's ratio of the material is taken to be 0.3, Young's modulus of the material is 3e7N/m^2.

Table 6: Nondimensional central deflection w_0/t of a clamped square plate subjected to a uniformly distributed load q.

q	w_0/t				
	2×2	4×4	6×6	8×8	Analytical
0.1	0.064352	0.064820	0.064958	0.065007	0.068374
0.2	0.128357	0.128924	0.129126	0.129197	0.135593
0.3	0.191685	0.191669	0.191800	0.191846	0.200683
0.5	0.315178	0.311175	0.310655	0.310470	0.322050
0.8	0.489526	0.472092	0.469447	0.468527	0.479763
1.3	0.746123	0.693022	0.685407	0.682812	0.688258
2.1	1.077707	0.958577	0.943137	0.937963	0.933327
3.4	1.479089	1.263356	1.238257	1.229945	1.214635
5.5	1.939395	1.601500	1.566364	1.554802	1.531733

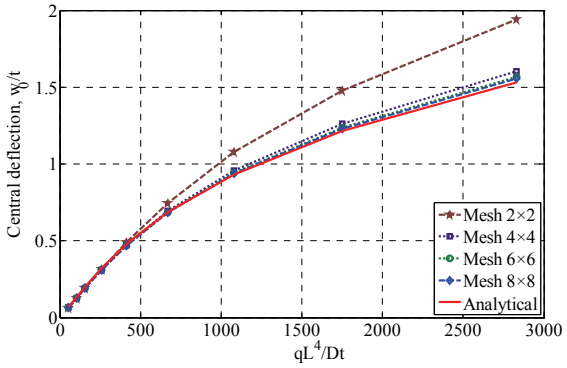

Figure 10: Nonlinear center deflection versus load for a clamped square plate subjected to a uniformly distributed load.

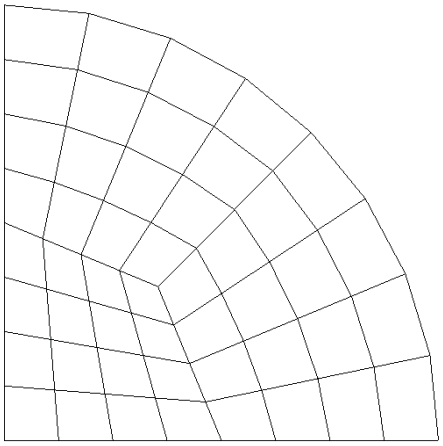

Figure 11: Configuration and mesh of a quadrant of a circular plate.

For linear analysis, the clamped circular plate subjected to uniform load q. The analytical solutions for deflections are given by Timoshenko and Woinowsky-Krieger (1940):

$$w = \frac{q}{64D}(R^2 - r^2)^2 \tag{53}$$

where r is the radial distance from the plate center, and $D = Et^3/\left(12\left(1-\nu^2\right)\right)$ is the bending stiffness.

Figure 12 shows the deflections along the radial line obtained from present method and the analytic solution computed by Eq. (53). It indicates that the present SFEM gives very accurate results.

For nonlinear analysis, the clamped circular plate with uniform loading q_0 is considered. The ana-

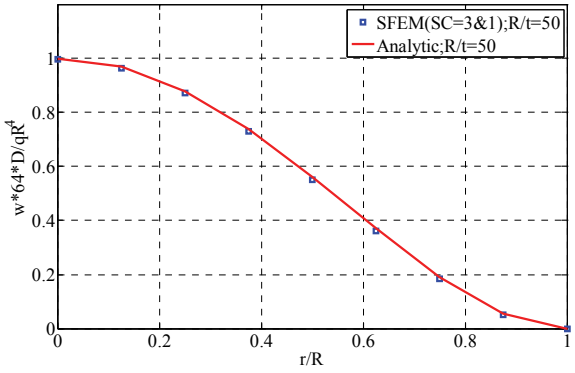

Figure 12: Deflection for the clamped circular plate subjected to uniform load along the radial line.

lytic central deflection is given by chia (1980):

$$\frac{qR^4}{Et^4} = \frac{16}{3(1-\nu^2)} \left[\frac{w_0}{t} + \frac{1}{360}(1+\nu)(173-73\nu)\left(\frac{w_0}{t}\right)^3\right] \quad (54)$$

where w_0 is the central deflection.

Figure 13 shows the load-deflection curves of the computed results by present method and analytic solutions calculated using Eq. (54). It can be observed that the present results agree well with analytic solutions.

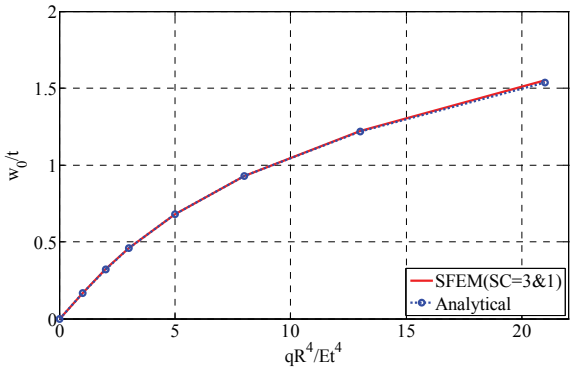

Figure 13: Nonlinear center deflection versus load for a clamped circular plate subjected to a uniformly distributed load.

4.3 Scordelis-Lo roof problem

The Scordelis-Lo roof shown in Fig. 14 is a famous benchmark problem for shell analysis to test a numerical method. The length of the shell is L=25ft, the radius is R=25ft, the thickness is t=0.25ft and the span angle is θ_0=40°. The material properties are: Poisson's ratio υ=0.3, and Young's modulus E=4.32e8N/ft^2. The boundary conditions at each end are supported by a rigid diaphragm. The loading is uniform vertical gravity load of q_0=90N/ft^2. Owing to the symmetry, only a quarter of the roof is modeled.

Several existing shell elements are used here to compare with the present method. They are 4-Node SRI (A standard 4-node Mindlin element with selective reduced integration) proposed by Hughes and Liu (1981), YASE (A 4-node shell element using one integration point and physical hourglass control) advanced by Engelmann and Whirley (1990), MITC4 (A 4-node fully integrated shell element using Mixed Interpolated Tensorial Components) proposed by Dvorkin and Bathe (1984), QPH (One point quadrature quadrilateral shell element with physical hourglass control) proposed by Belytschko and Leviathan (1994). The theoretical value 0.3024 of the vertical deflection at the centre of the free edge and the results of existing elements are obtained from Belytschko and Leviathan (1994). Table 7 shows the comparisons of the present result with solutions obtained by existing shell elements. It is observed that the present SFEM (SC=3&1) works very well.

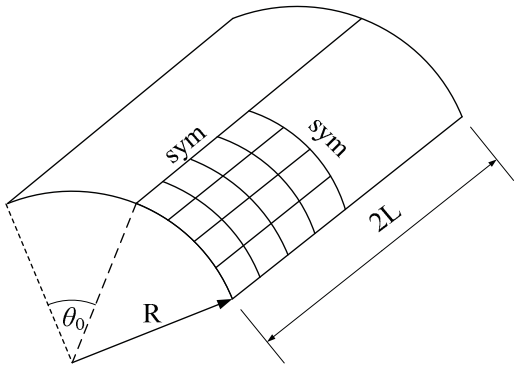

Figure 14: A quarter of a shell panel is meshed with quadrilateral elements.

4.4 Nonlinear analysis of shells

A cylindrical shell panel clamped along all four boundaries shown in Fig. 14 is now investigated for nonlinear analysis. The shell panel is subjected to uniform inward radial loading q_0. This example has been studied extensively by a number of researchers using the finite element methods. The geometry parameters of the panel are: L=254mm, R=2540mm, t=3.175mm and θ_0=0.1rad. The material properties are: υ=0.3 and E=3.10275kN/mm^2. Due to double symmetry of geometry and deformations, only one-quarter of the panel was discretized using a mesh of 8×8.

The present results of the center deflection, to-

Table 7: Scordelis-Lo roof (the value used for normalization is 0.3024)

Mesh	SFEM (SC=3&1)	4-node SRI	YASE	MITC4	QPH
4×4	1.04	0.96	1.05	0.94	0.94
8×8	0.99	0.98	1.01	0.97	0.98
16×16	1.01	1.00	1.02	1.00	1.01

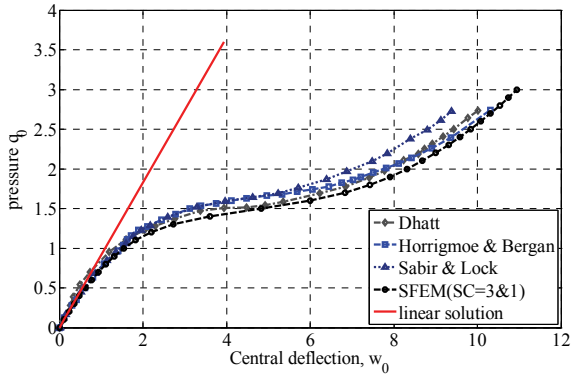

Figure 15: Nonlinear response of a clamped cylindrical shell panel to a uniformly distributed load.

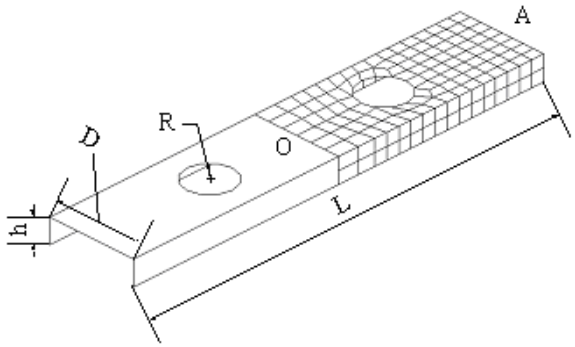

Figure 16: Model of a Reinforcing Plate of Automobile's Front Longeron.

gether with solutions given by Horrigmoe and Bergan (1978), Dhatt (1970) and Sabir and Lock (1973), are shown in Fig. 15. It is seen that the solutions agree well. The result using present SFEM (SC=3&1) is slightly bigger than others. It is confirmed that the stiffness of the SFEM model is softer than that of the FEM.

4.5 *Reinforcing Plate of Automobile's Front Longeron*

Finally, an actual structure component of a Reinforcing Plate of Automobile's Front Longeron with two fixed ends shown in Fig.16 is studied here using the present SFEM.The length is$L$=271mm, the length of the flanging is h=15mm, the width D=55.48mm, the radius of hole is R=15mm and the thickness is t=1mm. Poisson's ratio of the material is taken to be 0.3; Young's modulus of the material is E=2.1e5N/mm^2. The loading is uniform pressures on the surface which is q_0=0.01N/mm^2. Due to the symmetry, only half of the model is investigated with symmetry conditions applied on the nodes on the plane of symmetry.

We study this problem using the present SFEM (SC=3&1), and the FEM of quadrilateral element with reduced integration (Q4-R). The results of deflections along the line OA are plotted in Fig.17. The reference solutions are obtained using software *Altair OptiStruct* with large number of (22017) nodes. Fig.17 shows that the results using present method with 205 nodes is more close to the reference solutions.

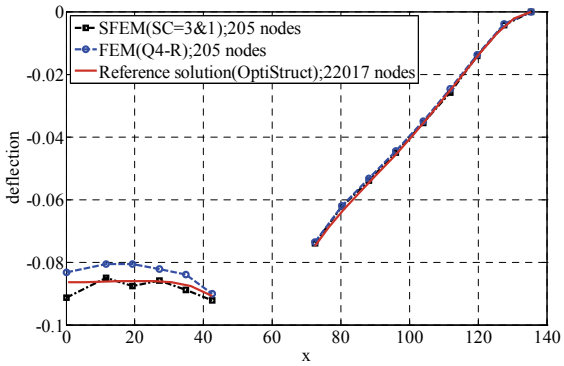

Figure 17: Deflection along the line OA (see Fig.16).

5 Conclusions

A novel Smoothed Finite Element Method (SFEM) using quadrilateral elements is presented in this paper to analyze linear and geometrically nonlinear problems of plates and shells. The effect of the number of smoothing cells in an element is investigated in detail. It is found that three smoothing cells for bending strain energy integration, and one cell for shear strain energy integration is the most preferred for analysis of plates and shells. The numerical examples reveal the following features of the present method:

(1) It uses strain smoothing technique that reduces the over-stiff phenomenon in the fully compatible displacement-based finite element.

(2) Area integration over each smoothing cells is recast into line integration along its edges, and hence no mapping is needed. This allows the use of extremely distorted elements.

(3) Shear locking phenomenon can be easily avoided by using only one smoothing cell for shear strain energy integration, and hence it works very well for both thick and thin plates and shells.

(4) Numerical results obtained from the SFEM are more accurate and the convergence is faster compare with the existing FEM elements.

(5) It works well for both linear and nonlinear problems.

Acknowledgement: The support of National Outstanding Youth Foundation (50625519), Key Project of National Science Foundation of China (60635020), Program for Changjiang Scholar and Innovative Research Team in University and the China-funded Postgraduates' Studying Aboard Program for Building Top University are gratefully acknowledged. The authors also give sincerely thanks to the support of Centre for ACES, Singapore-MIT Alliance (SMA), and National University of Singapore.

References

Atluri, S.N. (2004): *The Meshless Method(MLPG) for Domain & BIE Discretizations*, 680 pages, Tech Science Press.

Atluri, S.N. (2005): *Methods of Computer Modeling in Engineering & Sciences-I*, 625 pages, Tech Science Press.

Atluri, S.N; Han, Z.D.; Rajendran, A.M. (2004): A new implementation of the meshless finite volume method, through the MLPG "Mixed" approach, *CMES:Computer Modeling in Engineering & Sciences*, vol. 6, pp. 491-513.

Atluri, S.N.; Shen, S. (2002): *The Meshless Local Petrov-Galerkin (MLPG) Method*. 440 pages, Tech Science Press.

Basar, Y.; Kintzel1, O. (2003): Finite Rotations and large Strains in Finite Element Shell Analysis. *CMES: Computer Modeling in Engineering & Science*, vol.4, pp.217-230.

Bathe, K.J.; Dvorkin, E.H. (1985): A four-node plate bending element based on Mindlin–Reissner plate theory and mixed interpolation. *International Journal for Numerical Methods in Engineering*, vol. 21, pp. 367–383.

Batoz, J.L.; Tahar, M.B. (1982): Evaluation of a new quadrilateral thin plate bending element. *International Journal for Numerical Methods in Engineering*, vol. 18, pp. 1655–1677.

Belytschko, T.; Leviathan, I. (1994): Physical stabilization of the 4-node shell element with one point quadrature. *Computer Methods in Applied Mechanics and Engineering*, vol. 113, pp. 321-350.

Chen, J.S.; Wu, C.T.; Yoon, S.; You, Y. (2001): A stabilized conforming nodal integration for Galerkin meshfree methods. *International Journal for Numerical Methods in Engineering*, vol. 50, pp. 435-466.

Chen, X.L.; Liu, G.R.; Lim, S. P. (2003): An element free Galerkin method for the free vibration analysis of composite laminates of complicated shape, *Composite Structures*, vol. 59, pp. 279-289.

Chia, C.Y. (1980): *Nonlinear Analysis of Plate*. McGraw-Hill, New York.

Crisfield, M.A. (1997): *Non-Linear Finite Element Analysis of Solids and Structures*. Vol.1. Wiley: Chichester.

Dai, K.Y; Liu, G.R. (2007): Free and forced vibration analysis using the smoothed finite element method (SFEM). *Journal of Sound and Vibration*, vol. 301, pp. 803-820.

Dai, K.Y.; Liu, G.R.; Nguyen, T.T. (2007): An n-sided polygonal smoothed finite element method (nSFEM) for solid mechanics. *Finite Elements in Analysis and Design,* vol. 43, pp. 847-860.

Dhatt, G.S. (1970): Instability of thin shells by the finite element method, *IASS Symposium for Folded Plates and Prismatic Structures*, Vienna.

Dvorkin, E.N.; Bathe, K.J. (1984): A continuum mechanics based four-node shell element for general nonlinear analysis, *Engineering Computations*, vol. 1, pp. 77-88.

Engelmann, B.E.; Whirley, R.G. (1990): A new elasto-plastic shell element formulation for DYNA3D, *Lawrence Livermore National Laboratory*, Report UCRL-JC-104826.

Gu, Y.T.; Liu, G.R. (2001): A meshless local Petrov–Galerkin (MLPG) formulation for static and free vibration analyses of thin plates. *CMES: Computer Modeling in Engineering & Science*, vol. 2, pp. 463-476.

Horrigmoe, G.; Bergan, P.G. (1978): Nonlinear analysis of free-form shells by flat finite elements. *Computer Methods in Applied Mechanics and Engineering*, vol. 16, pp. 11-35.

Hughes, T.J.R.; Liu, W.K. (1981): Nonlinear finite element analysis shells: Part I, Three-dimensional shells. *Computer Methods in Applied Mechanics and Engineering*, vol. 26, pp. 331-362.

Jarak, T.; Sori? J.; Hoster, J. (2007): Analysis of shell deformation responses by the meshless local Petrov-Galerkin (MLPG) approach. *CMES: Computer Modeling in Engineering & Science*, vol.18, pp.235-246.

Lee, K.; Cho, C.; Lee S.W. (2002): A Geometrically Nonlinear Nine-Node Solid Shell Element Formulation with Reduced Sensitivity to Mesh Distortion. *CMES: Computer Modeling in Engineering & Science*, vol.3, pp.339-349.

Li, Q.; Soric, J.; Jarak, T.; Atluri, S.N. (2005): A locking-free meshless local Petrov-Galerkin formulation for thick and thin plates, *Journal of Computational Physics*, vol. 208, pp. 116-133.

Liu L.; Liu G.R.; Tan V.B.C. (2002): Element Free Method For Static And Free Vibration Analysis Of Spatial Thin Shell Structures. *Computer Methods In Applied Mechanics and Engineering*, vol. 191, pp. 5923-5942.

Liu, G. R. (2002): *Meshfree methods: Moving Beyond the Finite Element Method*, CRC Press: Boca Raton, USA.

Liu, G. R. (2008): A smoothed bilinear form for an alternative Galerkin formulation of solid mechanics problems. *International Journal of Computational Methods* (In press).

Liu, G.R.; Chen, X.L. (2001): A mesh free method for static and free vibration analyses of thin plates of complicated shape. *Journal of Sound and Vibration*, vol. 241, pp.839-855.

Liu, G.R.; Chen, X.L. (2002): Bucking Of Symmetrically Laminated Composite Plates Using the Element-Free Galerkin Method. *International Journal of Structural Stability and Dynamics*, vol. 2, pp. 281 – 294.

Liu, G.R.; Dai, K.Y.; Nguyen, T.T. (2007a): A smoothed finite element method for mechanics problems, *Computational Mechanics*, vol. 39, pp. 859-877.

Liu, G.R.; Quek, S.S. (2003): *The finite element method: a practical course*. Butterworth Heinemann, Oxford.

Liu, G.R.; Nguyen, T.T.; Dai, K.Y.; Lam, K. Y. (2007b): Theoretical aspects of the smoothed finite element method (SFEM). *International Journal for Numerical Methods in Engineering*, vol. 71, pp. 902-930.

Liu, G.R.; Zhao, X.; Dai, K.Y.; Zhong, Z.H.; Li, G.Y.; Han, X. (2008): Static and free vibration analysis of laminated composite plates using the conforming radial point interpolation method. *Composites Science and Technology*, vol. 68, pp. 354-366.

Long, S.R.; Atluri, S. N. (2002): A Meshless Local Petrov-Galerkin Method for Solving the Bending Problem of a Thin Plate. *CMES: Computer Modeling in Engineering & Science*, vol.3, pp.53-63.

Malkus, D.S.; Hughes, T.J.R. (1978): Mixed finite element methods - reduced and selective integration techniques: A unification of concepts. *Computer Methods in Applied Mechanics and Engineering*, vol. 15, pp. 63–81.

Nguyen-Van, H.; Mai-Duy, N.; Tran-Cong, T. (2008): A smoothed four-node piezoelectric element analysis of two- dimensional smart structures. *CMES: Computer Modeling in Engineering & Science*, vol.23, pp.209-222.

Nguyen-Xuan, H.; Rabczuk, T.; Bordas, S.; Debongnie, J.F. (2008): A smoothed finite element method for plate analysis. *Computer Methods in Applied Mechanics and Engineering*, vol. 197, pp. 1184-1203.

Qian, L.F.; Batra, R.C.; Chen, L.M.(2003): Elastostatic Deformations of a Thick Plate by using a Higher-Order Shear and Normal Deformable Plate Theory and two Meshless Local Petrov-Galerkin (MLPG) Methods. *CMES: Computer Modeling in Engineering & Science*, vol.4, pp.161-175.

Reismann, H. (1988): *Elastic Plates: Theory and Applications*. Wiley, New York.

Sabir, A.B.; Lock, A.C. (1973): The application of finite elements to the large deflection geometrically nonlinear behaviour of cylindrical shells. *International Conference on Variational Methods in Engineering*, Southampton, England; United Kingdom.

Sladek, J.; Sladek, V.; Wen, P.H.; Aliabadi, M.H. (2006): Meshless Local Petrov-Galerkin (MLPG) Method for Shear Deformable Shells Analysis. *CMES: Computer Modeling in Engineering & Sciences*, vol. 6, pp. 103-117.

Sori?J.; Li, Q.; Jarak, T.; Atluri, S.N. (2004): Meshless Local Petrov-Galerkin (MLPG) formulation for analysis of thick plates. *CMES: Computer Modeling in Engineering & Sciences*, vol. 6, pp. 349-357.

Suetake, Y. (2006): Plate Bending Analysis by using a Modified Plate Theory. *CMES: Computer Modeling in Engineering & Sciences*, vol. 11, pp. 103-110.

Timoshenko, S.; Woinowsky-Krieger, S. (1940): *Theory of Plates and Shells*. McGraw-Hill, New York.

Wang, D.D.; Chen, J.S. (2004): Locking-free stabilized conforming nodal integration for meshfree Mindlin-Reissner plate formulation. *Computer Methods in Applied Mechanics and Engineering*, vol. 193, pp. 1065-1083.

Wen, P.H.; Hon, Y.C. (2007): Geometrically Nonlinear Analysis of Reissner-Mindlin Plate by Meshless Computation. *CMES: Computer Modeling in Engineering & Sciences*, vol. 21, pp. 177-191.

Zienkiewicz, O.C.; Taylor, R.L. (2000): *The Finite Element Method*: The fifth edition, Vol 1: The Basis, Vol 2: Solid Mechanics, Butterworth-Heinemann.